JOURNAL OF AIRCRAFT
Vol. 30, No. 4, July–Aug. 1993

CFD Analysis of the X-29 Inlet at High Angle of Attack

R. H. Tindell* and W. G. Hill Jr.†
Grumman Corporation, Bethpage, New York 11714

This article presents the results of a computational fluid dynamics (CFD) analysis of the X-29 forebody inlet flowfield at high angles of attack and low speed. The goal of this work was to define the inlet performance and flow patterns, and identify any fluid dynamic mechanisms that could cause an unacceptable loss of performance or stability in the very high angle-of-attack operating regime, α = 50–90 deg, which has not yet been evaluated. External flow calculations to define inlet/forebody characteristics are done using a panel method; two-dimensional internal duct calculations employ a Navier-Stokes code. External and internal flow calculations are compared with wind-tunnel data, describing static and total pressure characteristics across a broad range of angle of attack. Computed inflow velocity patterns are also described and discussed. Results of a calculation describing inlet flowfield improvements provided by a slotted duct, demonstrate the application of CFD to efficiently screen innovative design modifications.

Nomenclature

A = area
CR = contraction ratio, $A_{\text{LEADING EDGE}}/A_{\text{MIN}}$
D_{CF} = compressor face diameter
FS = fuselage station
H = height
L = duct length
M = Mach number
Ps = static pressure
Pt = total pressure
R = denotes reattachment point
t = thickness
X = distance
α = angle of attack

Subscripts
C = capture
MIN = minimum
TH = throat
0 = freestream

Introduction

THE X-29 is a single engine forward-swept-wing technology demonstrator aircraft, having side inlets and a long duct that feeds a bifurcation just upstream of the F404-GE-400 engine. It was designed for efficient flight to Mo = 1.60 and for high angle-of-attack maneuvering down to low speeds. The inlet design has no moving parts, and capitalizes on efficient distribution of lip shape around the leading edge and the long duct, L/D = 7.2, to assure adequate performance and stability throughout its flight envelope, see Fig. 1.

The X-29 has successfully demonstrated all of its mission requirements, but it has not yet completed the low-speed high angle-of-attack program. It has demonstrated successful maneuvering operation to 50–60 deg angle of attack. Flight testing to angles of attack of 70–90 deg are anticipated.

Engine inlet performance has never been measured above α = 50 deg, which was the limiting wind-tunnel capability of a $\frac{1}{8}$-scale inlet-forebody model. The wind-tunnel data showed

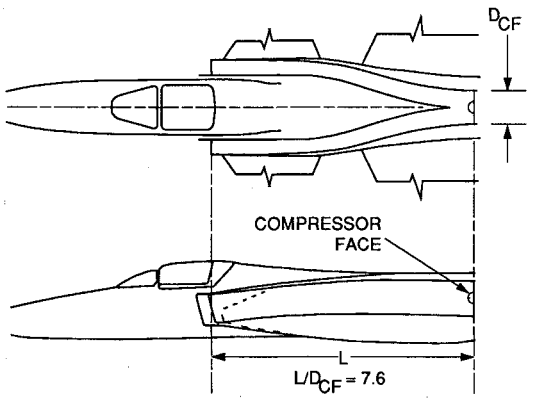

Fig. 1 X-29 inlet—aircraft arrangement.

well-behaved inlet operation, and implied efficient engine performance, up to α = 50 deg. Inlet-engine compatibility investigations by the Grumman/General Electric team, which applied the $\frac{1}{8}$-scale inlet data to engine stability analyses, showed no apparent problems. No flight test inlet instrumentation was employed. To bridge the gap between the wind-tunnel data base and the anticipated higher angle-of-attack flight test requirements, a computational fluid dynamics (CFD) analysis was conducted. The resources available were minimal. The goal was to uncover the presence of any adverse inlet flow phenomena that could either lead to engine surge or cause unacceptable loss of engine performance.

Inlet Design and Problem Definition

The X-29 inlet and its arrangement on the aircraft is described on Figs. 1 and 2. The splitter plate has an 8-deg wedge on its outboard side which generates an oblique shock for efficient supersonic operation. The long duct incurs fairly large friction losses, but assures good mixing characteristics that can attenuate flow distortions generated by lips and/or shock-boundary layer separation effects. Notice that the lower lip has thicker inboard sections to accommodate the higher local upwash due to the fuselage, at high angles of attack.

Figure 3 summarizes the internal cowl lip geometry relating to area contraction ratio. Definitions of local top, bottom, and side contraction ratios are given, and the result of the calculation of overall contraction ratio is shown to be CR = 1.186. More meaningful calculations of local top, side, and bottom lip contraction ratios are summarized in the other table on the figure. The bottom lip calculation is for the inlet vertical centerline geometry. Notice that the CR of the various

Received Sept. 30, 1991; revision received May 11, 1992; accepted for publication May 25, 1992.

*Principal Engineer, Grumman Aircraft Systems. Member AIAA.
†Staff Engineer, Grumman Aircraft Systems. Member AIAA.

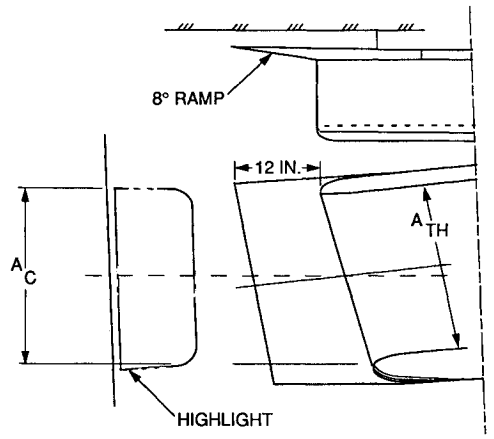

Fig. 2 X-29 inlet geometry.

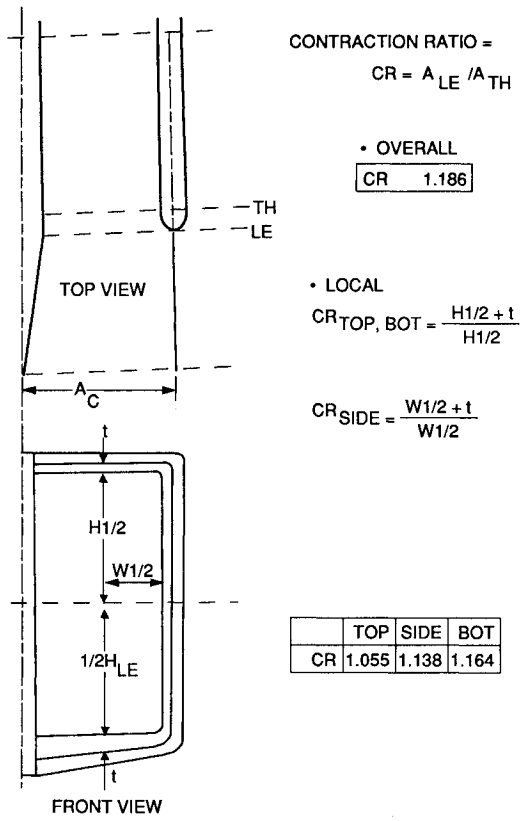

	TOP	SIDE	BOT
CR	1.055	1.138	1.164

Fig. 3 X-29 inlet contraction ratio characteristics.

sides are smaller than the overall calculation result. Although the bottom lip *CR* is the largest (1.164), and therefore, capable of higher angles of attack without incurring separation, it is characteristic of a relatively thin lip.

The effects of cowl lip contraction ratio on separation-free angle-of-attack capability are shown on Fig. 4, taken from Ref. 1. The figure reflects effects due to increasing angles of attack. The dashed lines, which represent VSAERO panel method calculations for two-dimensional inlets of various *CR* are compared with NASA test results,[2] for axisymmetric inlets. The reasonably close agreement of the *CR* = 1.37 test result with the *CR* = 1.35 calculation, especially at high throat Mach numbers, attests to the reasonable validity of the VSAERO model.

The X-29 lower lip's angle-of-attack capability has been estimated by locating the *CR* = 1.16 curve and entering it with a throat Mach number of 0.70, the X-29 design value. Lower lip separation is expected to occur at an angle of attack of 13 deg or greater. The side and top cowl lips, having smaller *CR*, would separate at lower values of their corresponding

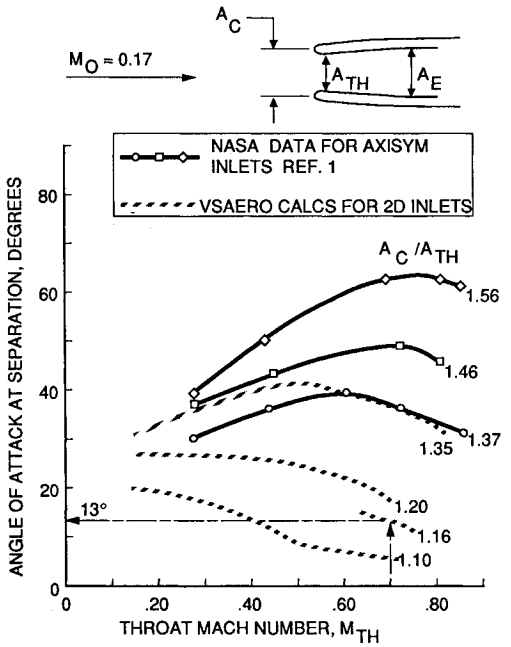

Fig. 4 Contraction ratio effects on internal lip separation.

inlet orientation (i.e., angles of yaw for the side lip and negative angle of attack for the top lip).

These results show that the X-29 inlet will operate (and has been operating successfully) with internal lower cowl lip separation throughout much of the angle-of-attack range thus far demonstrated in the flight program. The extent and severity of the separation increases with angle of attack. Since the X-29 may fly to very high angles of attack, possibly in the 70–90-deg range, it is important to take a closer look at the fluid mechanics of the X-29 inlet at these attitudes.

Approach

The primary goal of this work was the prediction of the effects of the vehicle's forebody on the inlet flowfield, and of the inlet itself on the flow quality delivered to the engine. However, available resources were not large and shortcuts in the analysis were taken. Two of the "work-horse" codes in the Grumman library were selected to calculate the external and internal flows. VSAERO is a three-dimensional linearized potential flow panel method, developed by Analytical Methods Inc., in Bellview, Washington. It is automatically coupled to a boundary-layer calculation, and is useful for calculating external, internal, and external-internal flows up to the point of separation. PARC is a three-dimensional flowfield simulation program based on the Reynolds Averaged Navier-Stokes equations. Program options allow the calculation of inviscid, laminar, or turbulent flows. Calculations of turbulent flows utilize an algebraic turbulence model derived from the Baldwin and Lomax model. In this present work, we have used PARC to model a turbulent two-dimensional flowfield.

The external flow calculations were done using VSAERO. The VSAERO model included simulation of the internal duct down to station 385. Although these internal inviscid calculations cannot model the separated flow expected, it was useful to compare them with the Navier-Stokes calculations which were done exclusively for the internal flow. Figure 5 shows the VSAERO model. The entire maximum allowable number of panels (3000) were used to accurately define a single side of the forward part of the aircraft. This precluded evaluating angle-of-yaw effects. The plan was to evaluate the three-dimensional flowfields at the inlet entrance station. Also, by running an isolated inlet model (see Fig. 5) at the same angle of attack as the fuselage-inlet model, the effects of the fuselage

on the local inlet cowl lip environment, i.e., upwash/outwash, could be determined.

An important difference between the actual aircraft and the VSAERO model is that the thin splitter plate that isolates the forebody upwash from the inlet, especially at high angles of attack, was not modeled with VSAERO. The fuselage-to-inlet step resulting from the VSAERO model could allow fuselage wash to enter the inlet, thus possibly giving erroneous results. Therefore, care must be taken in interpreting the effects of angle of attack on inlet approach flowfield characteristics, especially on the inboard sections of the inlet.

The internal flow, calculated by the PARC code, was modeled by a 51,000 grid point isolated two-dimensional duct having a length which is $\frac{2}{3}$ of the actual duct, not simulating the duct bifurcation, see Fig. 6. The duct exit station, X/L = 0.67, corresponds to fuselage station 468. This length was selected because it allows for a relatively small and more economical grid model, while containing most of the duct area diffusion. The two-dimensionality precluded the ability to simulate duct offset and secondary flow effects. A constant height section (not shown) was run for three duct heights downstream of station 468, to locate the exit boundary condition plane. This allowed a more uniform flow to be developed at the exit plane, thus precluding exit plane recirculation problems in the computational procedures.

The two-dimensional duct model reflects upper and lower wall shapes defined by a cutting plane along the vertical centerline. The foreshortened duct simulates 70% of the area diffusion, which includes the maximum diffusion rate corresponding to an equivalent conical diffuser of less than 1 deg. The duct exit Mach number for the analytical model was taken to be appropriately higher than the true duct exit Mach number, consistent with the model-to-actual area ratio.

The secondary flow induced by the duct offset (not simulated here) which will occur predominantly within the downstream merging section, will induce vortical flows which may tend to adversely affect engine face distortions. The presence of the engine face just downstream of the merging ducts, however, will mitigate against distorted engine face flow by imposing a near-constant static pressure field. Therefore, although a full three-dimensional analysis would be desirable, the two-dimensional assumption adapted for this investigation should allow useful and insightful results. The physical mechanism that dominates engine face total pressure characteristics at high angles of attack, i.e., the lip-boundary layer separation bubble, is maintained. Engine face total pressure distortion, however, cannot be accurately evaluated with this modeling approach. Also, the subsequent analysis will show that the foreshortened duct is too great a restriction for this study, because it precluded visibility of the downstream end of the separated zone at very high angles of attack. Nevertheless, this relatively economical modeling approach strikes a good balance between resource expenses and significant results.

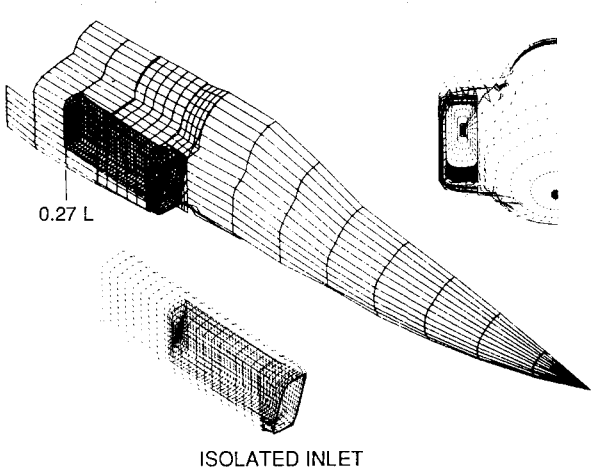

Fig. 5 VSAERO computational models.

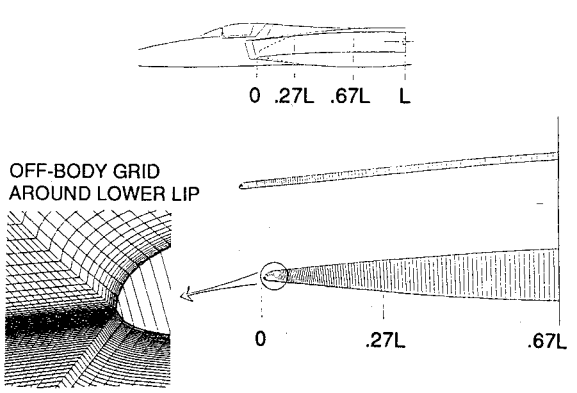

Fig. 6 Two-dimensional grid model for Navier-Stokes analysis.

Inlet test data from the $\frac{1}{8}$ scale wind-tunnel test,[3] were used to validate the computational results. The data include lip and duct static pressures and engine face total pressures over the angle-of-attack range of -10–49 deg. The engine face rake had 40 total pressure probes, 8 individual rakes (or spokes), each with 5 probes. Data were acquired at Mo = 0.15. All calculations in the present study were also done at Mo = 0.15.

The inlet airflow rate for this investigation is based upon the standard day maximum thrust operating condition of the F404-GE-400 engine, which corresponds to a throat Mach number of M_{TH} = 0.70.

Analysis

The effect of the fuselage on the inlet flowfield can be quantified by evaluating and comparing the local angle-of-attack profiles just upstream of the inlet station, for both the complete model and the isolated inlet of Fig. 5. Figure 7 shows the results of such a comparison for angles of attack of α = 10, 49, and 80 deg. The comparisons are made at station 320, which is 12 in. upstream of the bottom lip and 4.5 in. upstream of the top lip. The lower angle-of-attack calculations show close agreement across the central section of the inlets' projection, with a maximum variance between the two cases of approximately 3 deg, occurring across the bottom lip projection. The fuselage imposes a small upwash. A small asymmetry is seen as the result of the fuselage. The 49-deg angle-of-attack case shows a larger fuselage-induced upwash. A difference on the order of 10 deg occurs across the central section of the inlets' projection, with a smaller variation of approximately 6 deg in the projection of the bottom lip. At α = 80 deg we see a similar variation in local angle-of-attack characteristics between fuselage-inlet and isolated inlet. Calculations at other angles of attack have shown that the forebody upwash effect is approximately linear with angle of attack up to 49 deg and constant at higher angles of attack. It is concluded that no anomalous results are evident over the broad range of angles of attack from 0–80 deg.

Although VSAERO cannot calculate total pressure losses (inviscid and nonrotational flow only) calculations of internal cowl lip static pressures, when compared to test results, can indicate when separation occurs. Figure 8 compares the static pressures measured and calculated over the lower cowl lip at angles of attack of 0, 10, and 30 deg. The latter case has "plateaued" static pressure measurements that indicate separated flow occurring near the lip leading edge. A similar result was achieved at an angle of attack of 20 deg.

If we had test data at lower angles of attack, we could determine when separation occurred (the lowest angle at which a plateaued static pressure characteristic occurred). This should be close to α = 13 deg according to the result shown on Fig. 4. Unfortunately, data at angles of attack between 10 and 30 deg were not obtained. Therefore, we must use a calculation to estimate when separation first occurs. There is an iterative boundary-layer calculation available with VSAERO, but we

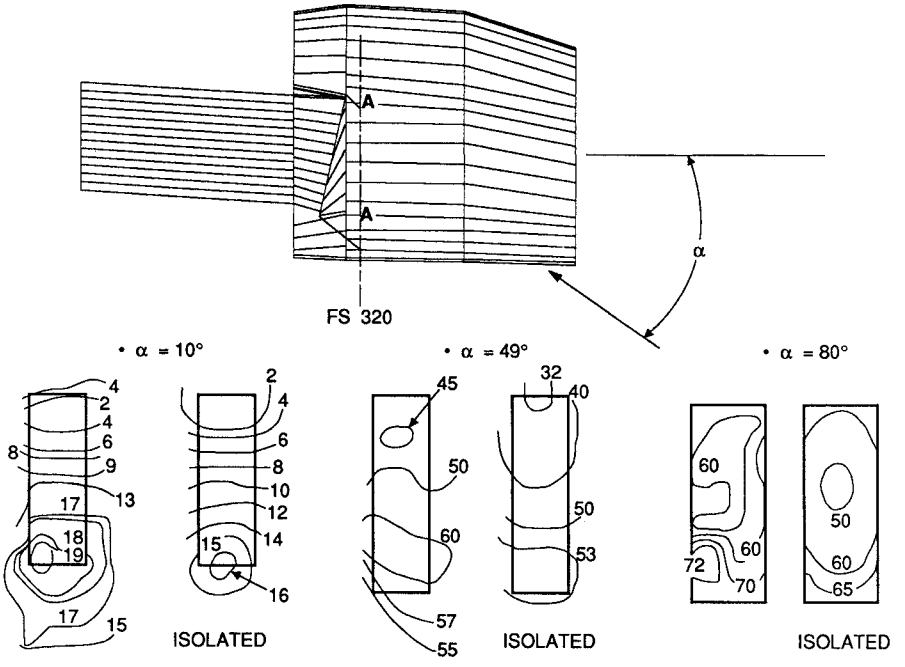

Fig. 7 Local angle-of-attack contours ahead of inlet.

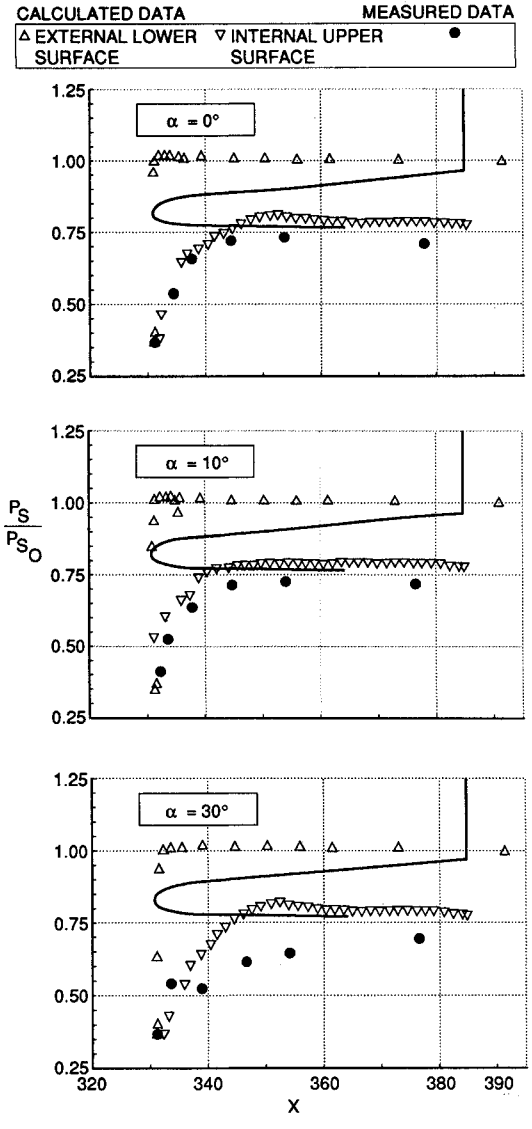

Fig. 8 VSAERO results: static pressure distributions.

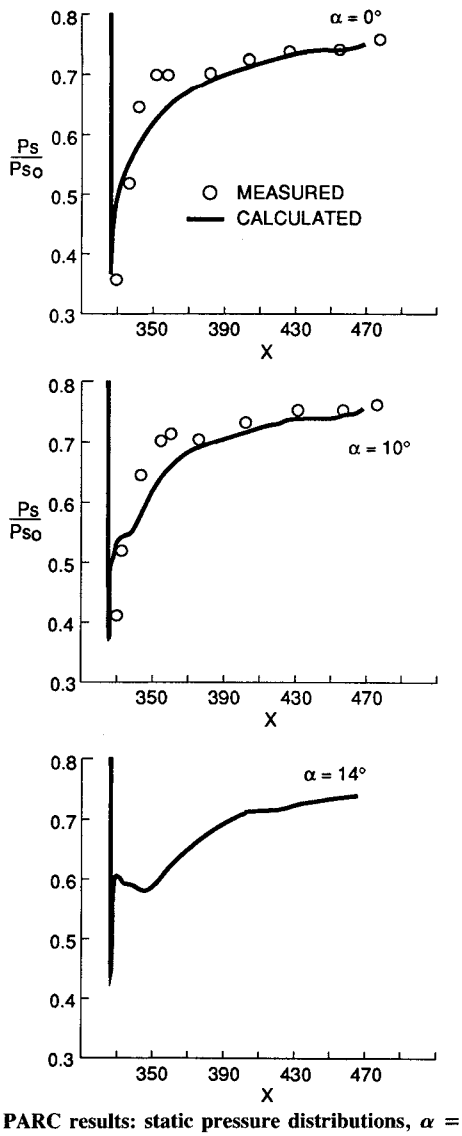

Fig. 9 PARC results: static pressure distributions, α = 0, 10, and 14 deg.

elected to use the PARC code to examine flow separation characteristics over the lower cowl lip. This allows concurrent calculation of the total pressure losses.

The two-dimensional isolated inlet model and lower lip grid arrangement developed for the PARC code are shown on Fig. 6. An appropriate static pressure boundary condition was imposed across the exit boundary condition plane to allow the same corrected airflow rate used in the VSAERO analysis. A comparison of calculated and measured lower lip static pressures at $\alpha = 0$ and 10 deg are presented on Fig. 9. Also shown is the calculation for $\alpha = 14$ deg. Good correlation between test and calculation is seen over the initial internal lip surface for both of the lower angle-of-attack cases. The calculations do not show the step compression and expansion seen in the test data within FS 340-370, although, as will be seen in Fig. 10, the calculations predict a separation and reattachment over the initial portion of the lip. Notice that the $\alpha = 10$-deg calculation shows a small plateau that could not be defined by the data because of too large a spacing of the pressure taps. The 14-deg calculation has no corresponding test data, but is useful because it shows a significant plateau just after the initial compression, similar to the $\alpha = 30$-deg data of Fig. 8. This tends to support the empirically derived verge of separation angle of attack of 13 deg for the X-29 lower lip (Fig. 4).

A more graphical understanding of the lower lip flow breakdown is provided on Fig. 10, which shows velocity and total pressure recovery fields within the inlet at 14-deg angle of attack. This angle is 1-deg greater than the angle at which the correlation of Fig. 4 predicted initial lower lip separation. The reattachment points are located by the symbol *R* on the velocity patterns. There are separation bubbles on both the upper and lower internal lips. The lower lip bubble is thicker and contains a larger region of low total pressure. At higher angles, the lower separation bubble will continue to increase, while the upper lip internal separation will be gone before 20 deg is reached.

Figure 11 plots the longitudinal station at which the calculation shows reattachment, thereby defining the length of the separation bubble over the complete angle-of-attack range. Separation is predicted downstream of our boundary condition exit station, FS 468, at angles of attack greater than 65 deg. By extrapolation, a bubble length 17% shorter than the length of the complete duct is indicated at 90 deg.

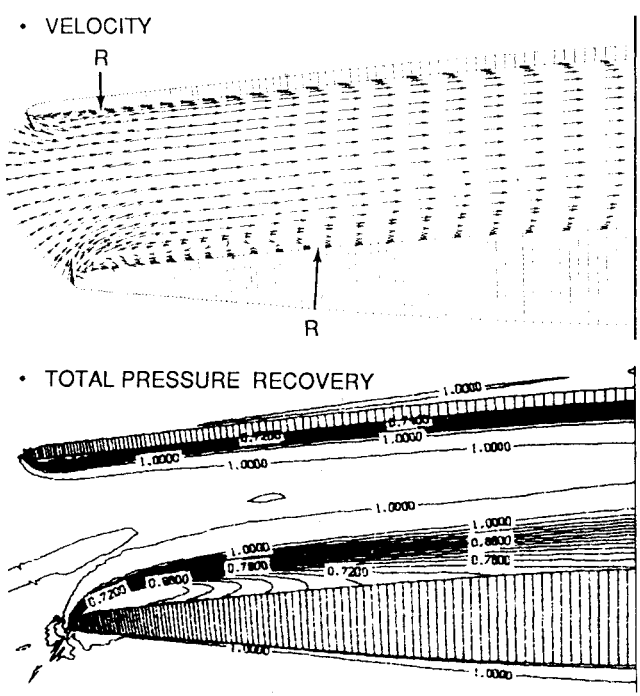

Fig. 10 Inlet characteristics at $\alpha = 14$ deg.

Total pressure recoveries at station 468 were determined by integrating the flowfield results across the station, for various angles of attack. Figure 12 shows the total pressure profiles over the angle-of-attack range of 10–90 deg. Notice that the lower half of the duct has almost all of the low quality flow, and that the maximum level is very close to 100% even at 90 deg. The area weighted averages of the profiles are plotted on Fig. 13, where they are compared with available test data. The test data are from a $\frac{1}{8}$ scale model and reflect an area weighted integration of a 40-probe engine face rake. Good agreement is achieved to 49 deg, and no precipitous drop-off is seen to 90 deg. Three-dimensional effects in the duct that were not modeled (such as crossflows induced by the high turning at the leading edge, and corner effects) are expected to be relatively small. Vortical effects resulting from

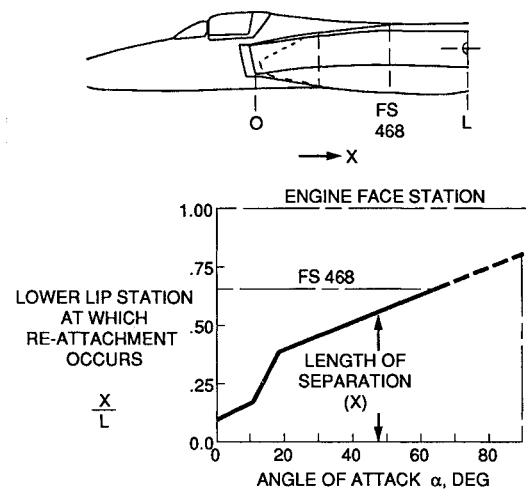

Fig. 11 Length of lower lip separation.

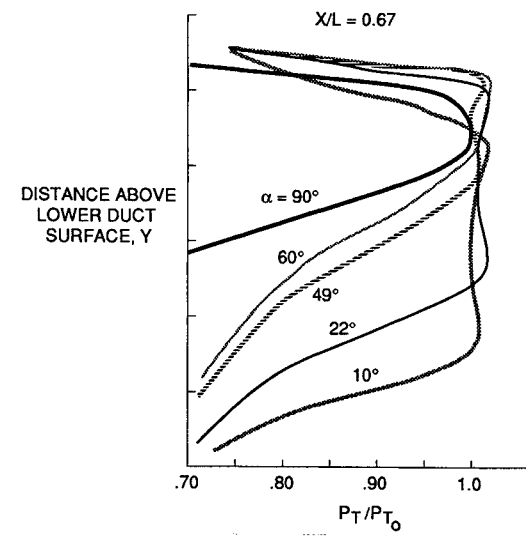

Fig. 12 Effects of angle of attack on total pressure profiles.

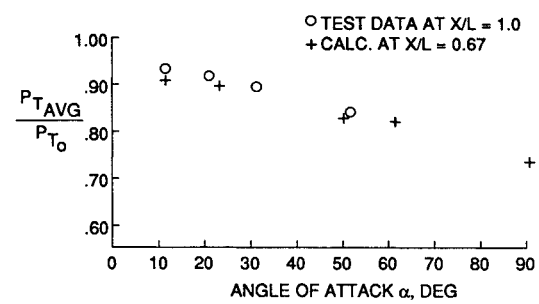

Fig. 13 Effects of angle of attack on average total pressure recovery.

secondary flows driven by duct curvature, predominantly in the duct-merging section, not simulated in this study, could be a source for additional total pressure losses. The good comparison with test results, however, suggests that the lower surface separation losses plus the normal wall boundary-layer losses dominated the overall performance, at least to 50 deg.

The test data revealed that the steady-state engine face total pressure distortion patterns were remarkably similar over a broad range of angle of attack. Figure 14 compares the total pressure patterns, $\Delta P_T/P_{T_{AVG}}$, at angles of attack of 10 and 40 deg. The lowest pressures are seen along both the duct wall and the symmetry plane boundary layers, consistent with classical fluid mechanical considerations. The intensities of the distortion patterns, defined by the overall distortion parameter, are also given on Fig. 14. An increase of 53% is incurred at the 40-deg angle-of-attack case. The lowest total pressures of this case, now shown on Fig. 14, occur at the bottom of the engine face.

An attempt was made to correlate the two-dimensional calculations at fuselage station 468 with the measured total pressure characteristics at the engine face station. The total pressure distributions along the median circumference of the engine face rake are compared with the calculated pressure distributions across the two-dimensional duct height at station 468 (see Fig. 15). Both angle-of-attack cases demonstrate a compensating trend that suggests that area weighted integrations of test and computed pressure distributions could yield similar average pressure recoveries, as was shown on Fig. 13. In both cases, the calculated results yield larger overall distortions than for the measured data. The minimum pressures calculated (lower surface) are lower than the corresponding test data, and the maximum calculated pressures are higher than their test counterparts. This denotes an apparent beneficial mixing effect not modeled in the calculations. It is interesting to note that the overall distortion parameters of the test data median circumference distributions of Fig. 15 show a reasonably close comparison to the values obtained from the complete engine face rake, Fig. 14.

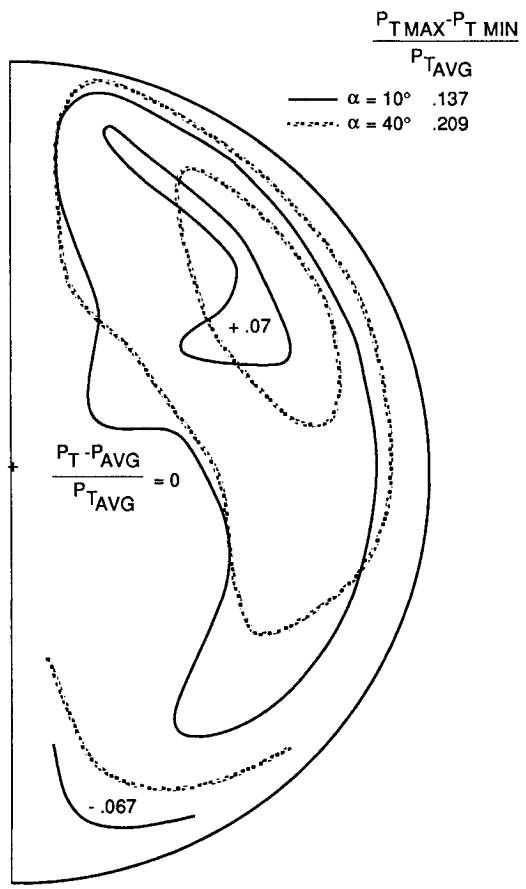

Fig. 14 Engine face total pressure distortion patterns (⅛-scale model data).

Inlet Modifications for High Angle-of-Attack Performance

A possibly effective means for improving the high angle-of-attack performance is to integrate a slot in the lower cowl that will induct high energy external air and merge it, tangentially, just upstream of the separation point. If sufficient momentum is transferred into the main inlet flow, separation can be precluded. The source of separation on the X-29 cowl is the lower cowl lip, and it is not practical to cut a slot through the thin leading edge. Alternatively, a slat may be fitted over the lip leading edge, as shown on Fig. 16. Off-design performance of such a slatted lip may be poor, especially if supersonic flight is required as with the X-29.

The same basic principle may be applied to a downstream station where there is ample cowl thickness for a slot. This approach is also shown in Fig. 16. Such a slot has been located at $X/L = 0.193$ on the X-29 lower cowl, which is where the external stagnation point is located at $\alpha = 49$ deg (Fig. 17). The slot exit height is 1.2 in., located at $X/L = 0.244$. The internal slot configuration, a step contour, does not reflect good design practice other than providing a tangential high energy stream. The step-contour was selected because it is coincident with the existing computational grid arrangement, and therefore, allowed a rapid and easy means to modify the local geometry from the original configuration. For application to an aircraft, a slot may require a hinged flap (Fig. 16) to preclude reverse flow.

Figure 17 shows the velocity field at an angle of attack of 49 deg. Notice that high energy slot flow causes reattachment of the separated flow by $X/L = 0.35$. This is a distance of 19 in. or 16 slot exit heights. An expanded view of the velocity field of the slotted configuration is compared with the un-

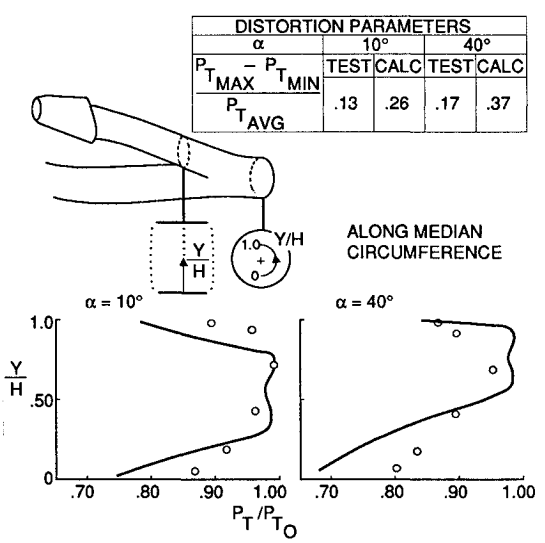

Fig. 15 Comparison of calculations at FS 468 with test data at engine face station, along median circumference.

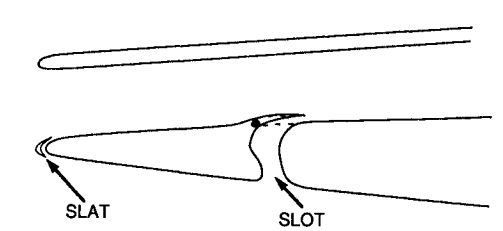

Fig. 16 Cowl modifications for improved high angle-of-attack performance.

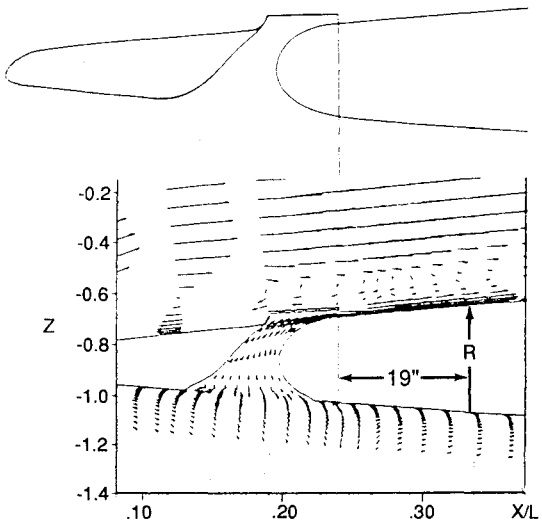

Fig. 17 Lower lip slot evaluation at α = 49 deg.

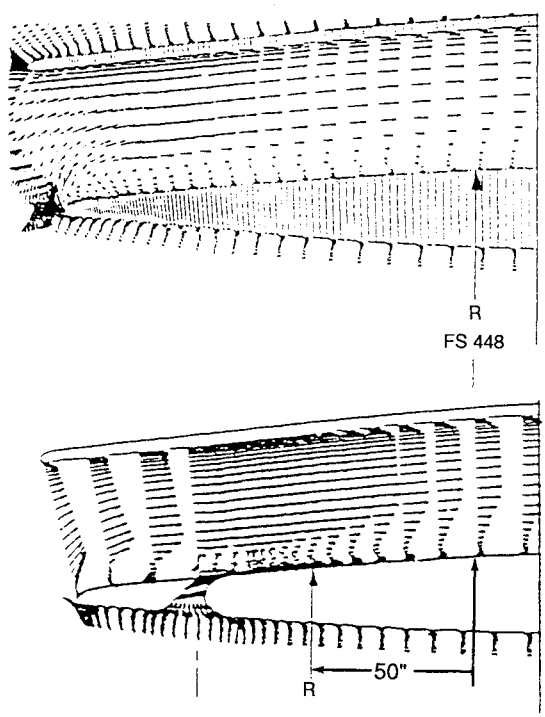

Fig. 18 Lower lip slot effectiveness at reducing reattachment α = 49 deg.

slotted configuration in Fig. 18. The slot flow has caused the reattachment point to move forward by 50 in. The subsequent effect on total pressure recovery is described in Fig. 19 which compares the profiles at X/L = 0.67, and also shows that the average total pressure recovery improvement due to the slot is 3% (from P_{T2}/P_{T0} = 0.837 to 0.863). Notice that the high total pressures of the slot case profile were extended into the lower section of the flow by about 14% of the duct height. These results could be improved upon by maximizing the slot's forward location in the duct and the size of the slot exit. The present results are intended only to show the practicality of such a device. If flight test results are warranted, a study to optimize a slot (or a slat) could be performed using the present results as a point of departure.

Conclusions

The X-29 air inlet system was numerically evaluated at *Mo* = 0.15 over an angle-of-attack range of 0–90 deg. The two CFD codes used were VSAERO, a linear aerodynamic panel method, and PARC, a full Navier-Stokes code. Limitations

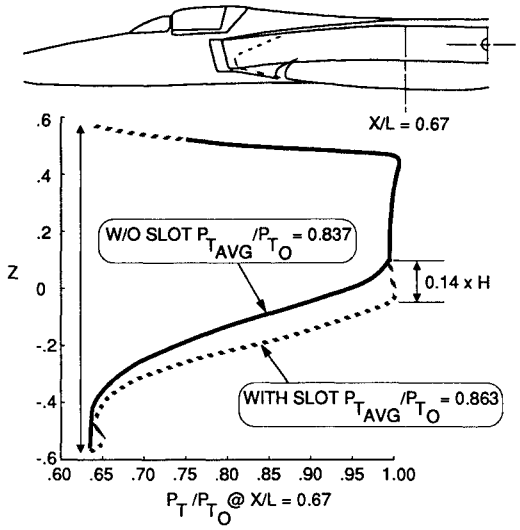

Fig. 19 Effect of slot on total pressure profile, α = 49 deg.

to the physical modeling were incurred because of code and computer resource restrictions. For example, the three-dimensional fuselage-inlet model of VSAERO, used to describe the external-internal flowfield, did not simulate the thin splitter plate and diverter channel that isolates the inlet from the fuselage upwash. Also, the PARC code was used to describe a two-dimensional model of the lip and (foreshortened) duct flowfield, rather than a three-dimensional one, to allow a relatively economical use of the CRAY computer.

Calculations, as well as correlations with NASA data and other work show that strong separation on the lower lip internal surface begins at an angle of attack of 13 deg. No adverse effects on engine operation have thus far been reported up to an angle of attack of 50 deg, the maximum angle flown thus far. This result is consistent with the inlet-engine compatibility work done by the Grumman-General Electric team using $\frac{1}{8}$-scale wind-tunnel model data. We conclude that the relatively long duct allows reattachment and sufficient mixing to maintain low engine face distortions.

The VSAERO calculations show a small fuselage-induced upwash, especially at angles of attack greater than 49 deg. The inlet splitter plate and diverter channel, not modeled by VSAERO, may isolate the inlet from the upwash.

The PARC calculations show the development of a lower surface separation bubble that begins at the internal lip surface and grows in length and height across the duct, as angle of attack is increased. The bubble is estimated to extend approximately 83% of the duct length at α = 90 deg. The calculated total pressure recoveries compare well with the measured wind-tunnel values over the range of available data ($\alpha \leq$ 50 deg), and show no precipitous drop-off up to α = 90 deg. These results suggest that there may be no impediment to compatible inlet-engine operation over the broad range of angle of attack investigated.

A calculation was performed to show the potential of locating a slot in the forward section of the lower duct, to energize the boundary layer, and thereby, improve high angle-of-attack performance. The slot was crudely configured to conform to the existing off-body grid, thereby saving modeling time and providing a conservative framework for the calculation. The slot's location and size were not optimized, but were selected based upon engineering judgment. Results showed that the separation bubble length was reduced by 40% at an angle of attack of 50 deg. A concurrent 3% increase in total pressure recovery was predicted.

These applications of CFD demonstrate two of the more significant uses for advanced aircraft development. The first is the ability to evaluate configurations that must be flown but cannot be tested in wind tunnels, as with the very high

angles of attack of the X-29 inlet system. The second is the ability to rapidly and inexpensively evaluate innovative modifications that can enhance performance, such as with the slot in the present inlet study. It is important to note that the slot evaluation showed a worthwhile performance improvement which can open the way for wind-tunnel development of a flight-worthy modification, if necessary. That is, the proper design process would be an efficient integration of CFD and experimental methods.

References

[1]Sandler, J. S., "A Preliminary Study of Two-Dimensional Subsonic Inlet Design for High Angle of Attack," Grumman Rept. PXT-001-77, Oct. 1985.

[2]Paul, D. L., "Quiet Clean Short-Haul Experimental Engine (QCSEE) Aerodynamic Characteristics of 30.5 cm Diameter Inlets," NASA CR-134866, Aug. 1975.

[3]Brown, N., "Interim Propulsion Analysis Report, Volume I," Grumman Rept. 712/ENG-RPT-82-020, Aug. 1982.